Redox Behavior of the Model Catalyst Pd/CeO2−x/Pt(111)

ARTICLE *in* THE JOURNAL OF PHYSICAL CHEMISTRY C · JULY 2008

Impact Factor: 4.77 · DOI: 10.1021/jp8004103

Redox Behavior of the Model Catalyst Pd/CeO_{2-x}/Pt(111)

E. L. Wilson,[†] R. Grau-Crespo,[†] C. L. Pang,[†,‡] G. Cabailh,[†,‡] Q. Chen,[†,‡,§] J. A. Purton,[||] C. R. A. Catlow,[†] W. A. Brown,[†] N. H. de Leeuw,[†] and G. Thornton*[,†,‡]

Department of Chemistry and London Centre for Nanotechnology, University College London, 20 Gordon Street, London WC1H 0AJ, U.K., and STFC Daresbury Laboratory, Warrington WA4 4AD, U.K.

Received: January 16, 2008; Revised Manuscript Received: April 8, 2008

Photoelectron spectroscopy and scanning tunneling microscopy have been used to investigate how the oxidation state of Ce in CeO_{2-x}(111) ultrathin films is influenced by the presence of Pd nanoparticles. Pd induces an increase in the concentration of Ce^{3+} cations, which is interpreted as charge transfer from Pd to CeO_{2-x}(111) on the basis of DFT+U calculations. Charge transfer from Pd to Ce^{4+} is found to be energetically favorable even for individual Pd adatoms. These results have implications for our understanding of the redox behavior of ceria-based model catalyst systems.

1. Introduction

Cerium dioxide is an important component in automobile catalytic converters. Its activity is thought to involve the storage and release of oxygen, which is promoted by noble metals such as Pd, Pt, and Rh.[1] Despite the importance of such processes, there is still relatively little understanding of the underlying promotion mechanism at the microscopic level. In particular, there is no consensus regarding the importance of redox processes of the noble metal and the ceria support. This can be seen in the varying conclusions of X-ray photoelectron spectroscopy (XPS) studies of Rh,[2] Pd,[3–5] and Pt[6] on oxide supports. For instance, XPS results for Rh on CeO_2 were interpreted as indicating reduction of the substrate by Rh-catalyzed desorption of surface oxygen atoms. In this earlier work, charge transfer from Rh to the oxide was discounted on the grounds that bulk Rh and CeO_2 have similar work functions.[2] Studies of Pd on Al_2O_3,[4] CeO_2,[5,7] and TiO_2[3] arrived at different conclusions: in some cases substrate reduction was identified, whereas in the others there was no evidence of charge transfer.

To address the charge-transfer issue in a convincing fashion, the present work employs a combination of XPS and density functional theory (DFT) calculations to follow the interaction of Pd with CeO_{2-x}(111). We deliberately studied ultrathin films of CeO_{2-x}(111) as the support in order to enhance the surface sensitivity of the XPS measurements, and we precharacterized the supported Pd clusters with scanning tunneling microscopy (STM). The XPS results evidence Pd-induced reduction of the CeO_{2-x} thin films, and the DFT calculations of Pd on CeO_{2-x}(111) confirm that this arises from charge transfer from the noble metal to the substrate. In a very clear way, these results demonstrate how the presence of metal nanoparticles affects the oxidation state of ceria and hence its ability to store oxygen, which is of primary importance for our understanding of the catalytic behavior of these systems.

* Corresponding author. E-mail: g.thornton@ucl.ac.uk. Telephone: +44(0)20 7679 7979.
[†] Department of Chemistry, University College London.
[‡] London Centre for Nanotechnology, University College London.
[§] Current address: Department of Chemistry, University of Sussex, Brighton BN1 9QJ, U.K.
[||] STFC Daresbury Laboratory.

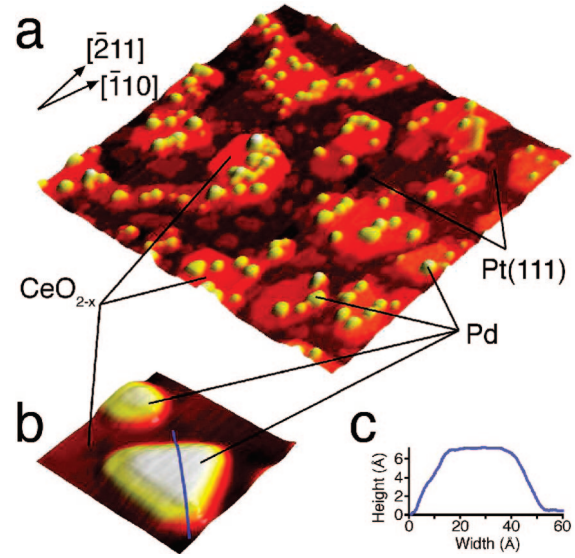

Figure 1. (a) (800 Å)^2 STM image of 0.2 MLE of Pd on Pt(111)—CeO_{2-x}, recorded with a sample bias of +3.6 V and a tunneling current of 1.0 nA. (b) (60 Å)^2 image of two of the larger Pd nanoparticles and (c) line profile over one of the nanoparticles in b, as indicated. The heights of the Pd nanoparticles range from 2 to 6 Å and the widths range from 5 to 30 Å.

2. Experimental and Computational Details

2.1. Experimental Details. The X-ray photoelectron spectroscopy (XPS) experiments were performed on an instrument described elsewhere,[7] operating at a base pressure of $\leq 2 \times 10^{-10}$ mbar. XPS data were recorded at room temperature using Mg Kα radiation ($h\nu$ = 1253.6 eV). The CeO_{2-x} thin films were grown in situ using a method described in detail elsewhere.[8] This method involves depositing cerium from an electron beam evaporator onto a clean Pt(111) surface at 300 K and then annealing to 1020 K for 3 min in ultrahigh vacuum. This gives rise to a (2 × 2) low-energy electron diffraction (LEED) pattern thought to indicate the formation of a Pt−Ce alloy.[8,9] Subsequent annealing to 1020 K for 3 min in an oxygen pressure of 1×10^{-5} mbar results in a CeO_{2-x}(111) thin film that gives rise to a (1.4 × 1.4) LEED pattern with respect to the LEED pattern for the clean Pt(111) surface. Previous scanning tunneling

10.1021/jp8004103 CCC: $40.75
Published on Web 06/26/2008

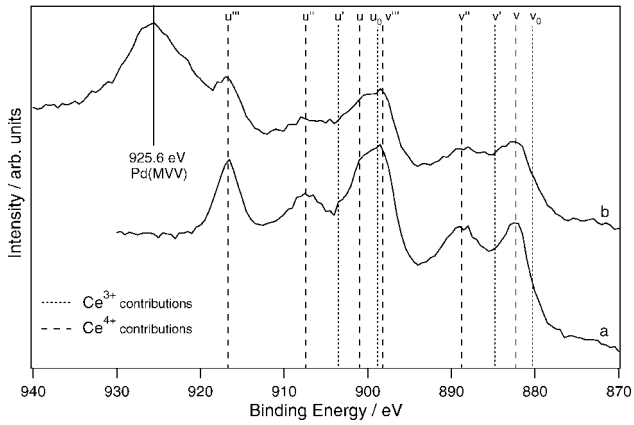

Figure 2. Ce 3d XPS spectra of a three-layer $CeO_{1.94}$/Pt(111) film (a) before and (b) after 10 MLE of Pd deposition at 300 K. Dashed lines indicate the location of Ce^{4+}-related peaks, and dotted lines indicate the location of Ce^{3+}-related peaks.

microscopy (STM) studies of CeO_{2-x} grown on Pt(111) have suggested that this growth method gives a surface structure consistent with oxygen-terminated fluorite-type CeO_2(111).[10] In XPS experiments, the thickness of the CeO_{2-x}(111) thin film was determined from the Pt 4f and Ce 3d photoemission intensities, using the method devised by Seah et al.[11] On this basis, the films investigated in all XPS experiments were three CeO_2 trilayers thick. The STM images were recorded with an Omicron GmbH variable-temperature instrument with a base pressure of $\sim 1 \times 10^{-10}$ mbar operated at room temperature. LEED and Auger spectroscopy, as well as STM, were used to check surface cleanliness and ordering. All images presented were recorded using a tungsten tip in the constant-current mode with a positive sample bias. For both the XPS and STM measurements, Ce was deposited from wires (99.95% purity) using metal evaporators, with O_2 (99.99% purity) admitted through a high-precision leak valve. Pd was deposited from an electron beam evaporator onto the sample at 300 K in ultrahigh vacuum.

2.2. Calculations. The spin-polarized density functional theory (DFT) calculations simulated the CeO_2(111) surface using O-terminated slabs containing nine atomic layers (three O—Ce—O trilayers) in the direction perpendicular to the surface, each slab being separated from the next by a vacuum gap of ~15 Å. The thickness of the slab corresponds to that of the experimental thin films described above. Parallel to the surface, the supercell consists of a 2×2 array of hexagonal surface unit cells. The calculations were performed using the DFT program VASP.[12–15] We used an exchange correlation functional built from the Perdew and Zunger[16] local functional, with the spin interpolation formula of Vosko et al.[17] and the gradient corrections by Perdew et al.[18] Wave functions were expanded in plane waves with a cutoff energy of 415 eV. The interaction between the valence electrons and the core was described with the projected augmented wave method.[19,20] To properly describe the localization of electrons on Ce 4f levels, orbital-dependent corrections using the DFT+U method were introduced.[21,22] A Hubbard parameter of $U_{\text{eff}} = 5$ eV was used. This is the value employed in other studies of ceria surfaces,[23] as well as that recommended by Andersson et al.[24] on the basis of a systematic study of reduced cerium oxides.

The inclusion of the Hubbard correction slightly increases the equilibrium cell parameter of cubic CeO_2 from 5.466 to 5.480 Å. Including the Hubbard correction does not modify the electronic structure significantly, because, to a first approximation, the f levels are empty in the unreduced oxide. (In practice, there is some occupancy of the f levels, which accounts for the small effects observed on the CeO_2 structure.) Hence, the effect of the Hubbard correction is important only when dealing with the reduced Ce^{3+} species. Similar arguments apply to the band gap of CeO_2, where we find a surface (O 2p)−(Ce 4f) band gap of 2.2 eV when including the *U* correction, which compares to the bulk band gap of 1.7 eV obtained by Loschen et al.[25] with the same method and value of *U*. Detailed discussions of the effects of the Hubbard correction on the calculated properties of cerium oxides, including the lattice constants and band gaps, can be found elsewhere.[24–26]

3. Results and Discussion

STM was used to characterize the morphology of Pd nanoparticles deposited on CeO_{2-x}(111) ultrathin films, and XPS was used to monitor the Pd-induced modification of the electronic structure. DFT calculations were carried out to determine the origin of the observed changes in electronic structure.

3.1. Structural Characterization. Figure 1 shows an STM image of CeO_{2-x}(111) thin film islands on Pt(111) after deposition of about 0.2 monolayer equivalents (MLE) of Pd. Here, one monolayer is defined as the number of Pt atoms in the top layer of Pt(111), and 1 MLE is the number of monolayers that would be formed if close-packed Pd atoms uniformly covered the substrate. STM reveals that the (111)-oriented film grows as flat-topped islands with an apparent thickness of between 3 and 4 Å, corresponding to one O—Ce—O trilayer. The island edges are aligned with Pt(111) principal azimuths, as expected from the alignment of LEED beams. Thinner islands (~2 Å thick) are also seen both directly on Pt(111) and connected around parts of the perimeters of the thicker CeO_{2-x} islands. Because Pd does not grow on these thinner islands, they probably consist of a less oxidized CeO_{2-x} phase. Moreover, it is clear that Pd grows preferentially on the terraces of CeO_{2-x} islands rather than at step edges or uncovered areas of the Pt(111) substrate. The latter observation was confirmed by evaporating Pd in situ while imaging with STM: no changes were observed over the Pt substrate while particles appeared on the CeO_{2-x} islands up to a coverage of 0.2 MLE. This is important, as it indicates that the XPS results are not modified by Pd−Pt(111) interactions, at least not in the coverage range explored with STM. Pd clusters vary in size from 5 to 30 Å diameter with a height range of 2−6 Å. The larger nanoparticles have atomically flat (111) top facets, as expected from a previous reflection−absorption infrared spectroscopy (RAIRS) study.[8] Our STM results for Pd on CeO_{2-x}(111) appear to be slightly different from those reported for a CeO_{2-x}(111) film grown on Ru(0001),[5] in that some preference for step-edge decoration was evidenced in the earlier work. This difference could arise from a number of factors, such as the defect density and the Pd flux employed.

3.2. Electronic Structure. Ce 3d XPS was used to monitor the Ce^{3+} concentration in the CeO_{2-x}(111) film using an established procedure.[8,9] The Ce 3d spectra consist of 10 Gaussian functions that can be assigned to either a Ce^{3+} or Ce^{4+} origin, hence allowing determination of the CeO_{2-x} stoichiometry. Figure 2 shows Ce 3d spectra for a three-layer CeO_{2-x}/Pt(111) film before and after deposition of 10 MLE of Pd. Fitting of the Ce 3d spectra reveals that the as-deposited CeO_{2-x} films consistently contain $(12.5 \pm 0.4)\%$ Ce^{3+} ($CeO_{1.94}$). Depositing 1 MLE of Pd increases the Ce^{3+} concentration of the $CeO_{1.94}$ film to $(20.9 \pm 0.7)\%$, and the concentration then remains

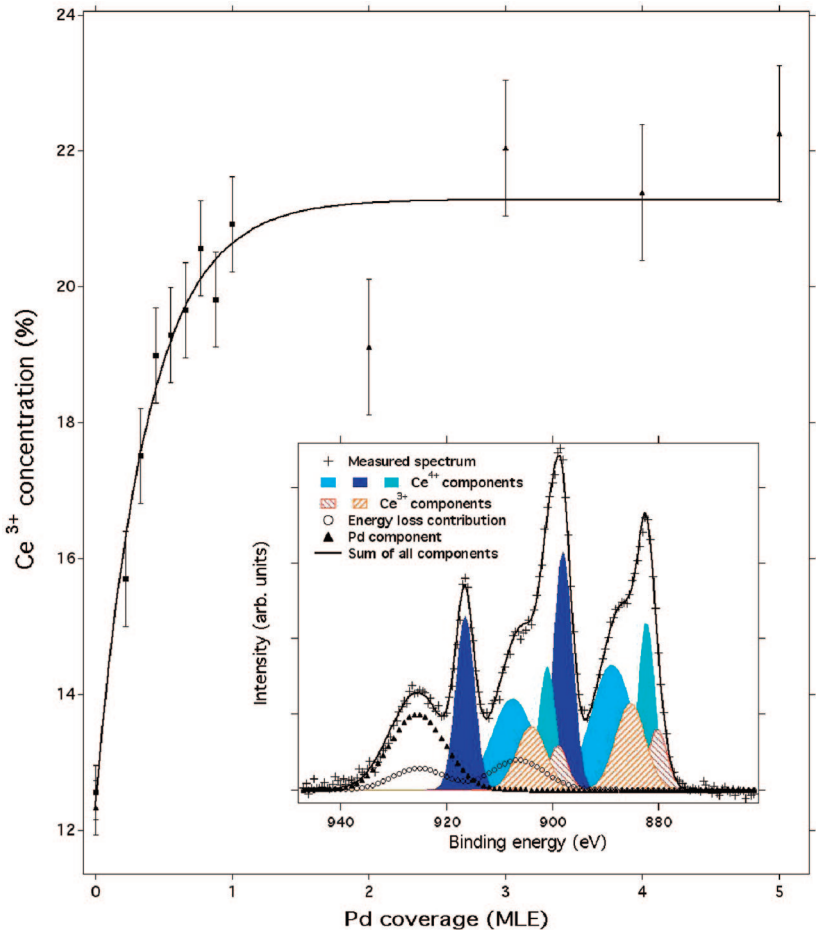

Figure 3. Ce^{3+} concentration of a three-layer $CeO_{1.94}(111)$ film as a function of Pd coverage. The percentage Ce^{3+} concentration was calculated by fitting Ce 3d XPS spectra with three doublet contributions from Ce^{4+} (blue), two from Ce^{3+} (red hashed), and one from energy-loss contributions (open circles). An example fit for the spectrum at 1 MLE Pd coverage is shown in the inset. One peak was used to fit the Pd MNN Auger peak (solid triangles). Binding energies and fwhm of all peaks were held constant for all fits.

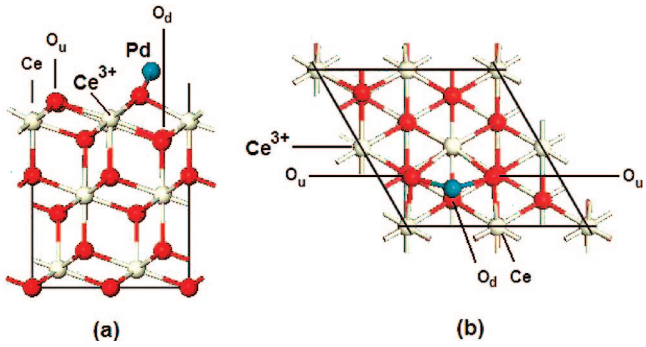

Figure 4. (a) Side and (b) top views of the unit cell employed in the DFT calculations, with a Pd atom adsorbed at its most stable position. Figure 3a also identifies the three high-symmetry adsorption sites on this surface: Ce cations; O_u (up), the outmost oxygen; and O_d (down), the subsurface oxygen atom in the top CeO_2 trilayer. The Ce site to which an electron is transferred is labeled Ce^{3+}. The O 2p band, the upper edge of which lies 2.2 eV below the Ce 4f lower band edge in the calculations for $CeO_2(111)$, is not shown.

constant at (21.2 ± 1.0)% for subsequent Pd doses above 2 MLE, as shown in Figure 3. The inset in Figure 3 shows the least-squares fit to a Ce 3d spectrum of a $CeO_{1.94}$ film. The Ce^{4+} and Ce^{3+} contributions were fitted with three and two Gaussian doublets, respectively, as described in previous work.[7,9] Satellites and a polynomial plus Shirley background were subtracted prior to the fit. The peak widths, branching ratio, and spin−orbit splitting were kept constant throughout. The binding energies were measured at 880.1 ± 0.5 and 885.4 ± 0.5 eV for the Ce^{3+} contributions and at 882.2 ± 0.6, 888.8 ± 0.7, and 897.9 ± 0.4 eV for the Ce^{4+} contributions (binding energies are given for the $3d_{5/2}$ peaks). The values of the spin−orbit splitting and branching ratio for all doublets were 18.6 ± 0.1 eV and 0.73, respectively. The Pd MNN Auger contribution, which overlaps with the high-binding-energy end of the spectrum, was fitted with one Gaussian peak. One extra doublet was added to the fits in addition to those employed in earlier work.[7,9] It is also split by 18.6 eV, with a binding energy for the $3d_{5/2}$ component of 906.5 ± 1.0 eV. This doublet most probably represents an energy-loss feature. These peaks have been observed in previous studies but not included in the analysis.[27]

The O KLL Auger peak was also monitored during Pd deposition using XPS (not shown), the Auger peak being used in preference to the O 1s XPS peak because the latter overlaps Pd features. The Ce 3d XPS/O KVV Auger intensity ratio was found to remain constant with increasing Pd coverage within the error bars. Pd 3d XPS spectra were also monitored. The Pd $3d_{5/2}$ peak appeared at 335.2 eV binding energy, independent of the Pd coverage, consistent with the value expected for metallic Pd.[28] Taken together, the XPS results are consistent with charge transfer from the Pd nanoparticles to the $CeO_{2-x}(111)$ film, where the hole in the nanoparticles is delocalized. This would explain the absence of a clear chemical shift in the Pd 3d XPS results.

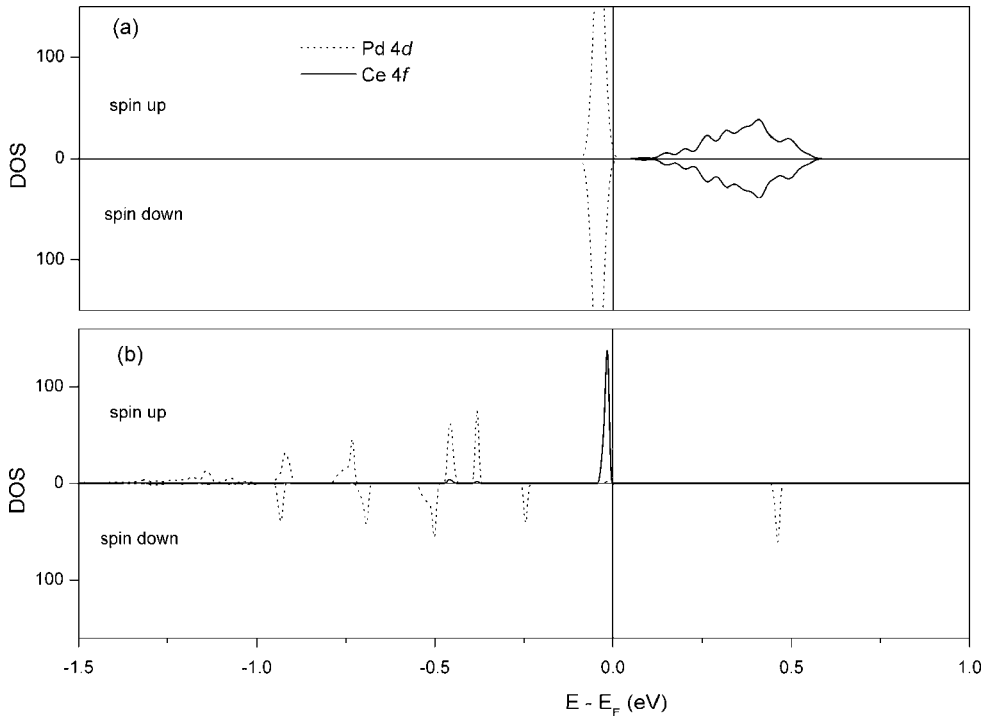

Figure 5. Electronic density of states projected onto the Pd 4d orbitals and the 4f orbitals of a surface Ce cation (a) before adsorption (Pd atom in the middle of the vacuum gap) and (b) after adsorption with charge transfer.

The data in Figure 3 are strikingly different from the XPS results of Senanayake et al.,[5] who found no evidence of Pd-induced reduction of thin film CeO_{2-x}(111) grown on Ru(0001). A likely explanation for this difference lies in the thickness of the ceria films employed. The earlier work employed a film about 50 Å thick,[5] substantially more than that investigated here. As noted above, we deliberately studied an ultrathin film in order to maximize the surface sensitivity of the XPS measurements.

3.3. DFT Calculations. We turn to DFT calculations to provide an explanation for the Pd-induced reduction of the CeO_{2-x}(111) film. To simplify the calculations, we investigated the interaction of a single Pd atom with CeO_2(111), looking in detail at three high-symmetry sites (see Figure 4). Other less symmetric sites, such as bridging positions between O_u and Ce, were also considered and found to be unstable. The lowest-energy (−1.91 eV) adsorption site is close to the O_d site, but is not completely symmetrical (see Figure 4). In this configuration, there is charge (electron) transfer from the Pd atom to the surface. This is similar to the result obtained by Yang et al. for the Pt—CeO_2(111) interface.[29] However, in contrast with their results, we found here that the electron donated by the Pd adatom is well localized on one particular Ce atom at the surface (identified as Ce^{3+} in Figure 4). Analysis of the projection of the spin density onto spherical harmonics shows that the unpaired electron in this Ce atom is localized on an f orbital, as expected for a Ce^{3+} cation (the integration of the spin density corresponding to this orbital is 0.97). The projected electronic density of states (DOS) for this lowest-energy solution (Figure 5) also shows very clearly that one of the Pd d levels is now empty and one f level of the Ce lies below the Fermi energy. The DOS peak just below the Fermi level is of pure Ce 4f character, with no significant mixing with orbitals of other surface atoms (e.g., O 2p levels) being found. Here, there are two unpaired electrons per unit cell, which reside on the Ce^{3+} and Pd^{+} atoms. The adsorption geometry (Figure 4) is such that the oxygen anions between Pd^{+} and Ce^{3+} move away from the reduced Ce^{3+} cations to be closer to the oxidized Pd^{+} species, as expected from the balance of electrostatic forces. The positions of the Ce atoms at the surface remained practically unaltered upon Pd deposition. Other stable adsorption sites are found in the absence of charge transfer, but they all have higher adsorption energies (−1.16 eV, −1.52 and −1.75 eV at the Ce, O_u and O_d sites, respectively). It is important to note that a low-energy adsorption site involving charge transfer is found with DFT only if a Hubbard correction (DFT+U) is included. Hence, earlier DFT calculations of Pd on ceria do not predict charge transfer.[30]

Finally, we should stress that in our calculations we did not consider possible effects arising from the presence of the metallic substrate. As some authors have already noted, some interactions, including charge transfer, can occur between the metallic substrate and species deposited at the free surface of an ultrathin oxide film.[31,32] Further work would clearly be desirable to investigate the presence of these interactions in the Pd/CeO_2/Pt(111) system.

4. Summary

XPS in conjunction with first-principles DFT calculations has been used to explore the idea that nanoparticles of noble metals could modify the Ce oxidation state in CeO_{2-x}. This is of relevance to the use of noble metals supported on CeO_{2-x} in automobile exhaust catalysts. The results indicate that Pd nanoparticles induce an increase in the number of Ce^{3+} cations. For a three-layer-thick $CeO_{1.94}$(111) film on Pt(111) (where each layer comprises an O—Ce—O trilayer), 1 MLE of Pd increases the Ce^{3+} concentration from 12.5% ± 0.4% to 21.2% ± 1.0%. DFT calculations confirm that charge transfer from Pd to Ce^{4+} is energetically favorable. Together, these results support a redox mechanism for noble-metal promotion of ceria in automobile catalysis.

Acknowledgment. We thank Matt Watkins for useful discussions. This work was funded by the EPSRC, with access to

HPCx computer resources provided via the Materials Chemistry Consortium (EPSRC Portfolio Grant EP/D504872/1).

References and Notes

(1) Trovarelli, A. *Catalysis by Ceria and Related Materials*; Imperial College Press: London, 2000; Vol. 2.
(2) Pfau, A.; Schierbaum, K. D.; Gopel, W. *Surf. Sci.* **1995**, *331−333*, 1479.
(3) Diebold, U.; Pan, J.-M.; Madey, T. E. *Surf. Sci.: Proc. 14th Eur. Conf. Surf. Sci.* **1995**, *331−333*, 845–854.
(4) Ealet, B.; Gillet, E. *Surf. Sci.* **1993**, *281*, 91–101.
(5) Senanayake, S. D.; Zhou, J.; Baddorf, A. P.; Mullins, D. R. *Surf. Sci.* **2007**, *601*, 3215.
(6) Schierbaum, K. D.; Fischer, S.; Torquemada, M. C.; de Segovia, J. L.; Roman, E.; Martin-Gago, J. A. *Surf. Sci.* **1996**, *345*, 261–273.
(7) Wilson, E. L.; Chen, Q.; Brown, W. A.; Thornton, G. *J. Phys. Chem. C* **2007**, *111*, 14215–14222.
(8) Wilson, E. L.; Brown, W. A.; Thornton, G. *Surf. Sci.* **2006**, *600*, 2555–2561.
(9) Schierbaum, K. D. *Surf. Sci.* **1998**, *399*, 29.
(10) Berner, U.; Schierbaum, K.-D. *Phys. Rev. B* **2002**, *65*, 235404.
(11) Seah, M. P. In *Practical Surface Analysis—Auger and X-ray Photoelectron Spectroscopy*; Briggs, D., Seah, M. P., Eds.; Wiley: New York, 1983; Vol. 1, pp 201−255.
(12) Kresse, G.; Furthmuller, J. *Comput. Mater. Sci.* **1996**, *6*, 15–50.
(13) Kresse, G.; Furthmuller, J. *Phys. Rev. B* **1996**, *54*, 11169–11186.
(14) Kresse, G.; Hafner, J. *Phys. Rev. B* **1993**, *48*, 13115–13118.
(15) Kresse, G.; Hafner, J. *J. Phys.: Condens. Matter* **1994**, *6*, 8245–8257.
(16) Perdew, J. P.; Zunger, A. *Phys. Rev. B* **1981**, *23*, 5048–5079.
(17) Vosko, S. H.; Wilk, L.; Nusair, M. *Can. J. Phys.* **1980**, *58*, 1200–1211.
(18) Perdew, J. P.; Chevary, J. A.; Vosko, S. H.; Jackson, K. A.; Pederson, M. R.; Singh, D. J.; Fiolhais, C. *Phys. Rev. B* **1992**, *46*, 6671–6687.
(19) Blochl, P. E. *Phys. Rev. B* **1994**, *50*, 17953–17979.
(20) Kresse, G.; Joubert, D. *Phys. Rev. B* **1999**, *59*, 1758–1775.
(21) Liechtenstein, A. I. *Phys. Rev. B* **1995**, *52*, R5467−R5470.
(22) Dudarev, S. L.; Botton, G. A.; Savrasov, S. Y.; Humphreys, C. J.; Sutton, A. P. *Phys. Rev. B* **1998**, *57*, 1505–1509.
(23) Nolan, M.; Grigoleit, S.; Sayle, D. C.; Parker, S. C.; Watson, G. W. *Surf. Sci.* **2005**, *576*, 217–229.
(24) Andersson, D. A.; Simak, S. I.; Johansson, B.; Abrikosov, I. A.; Skorodumova, N. V. *Phys. Rev. B* **2007**, *75*, 035109.
(25) Loschen, C.; Carrasco, J.; Neyman, K. M.; Illas, F. *Phys. Rev. B* **2007**, *75*, 035115.
(26) Da Silva, J. L. F.; Ganduglia-Pirovano, M. V.; Sauer, J.; Bayer, V.; Kresse, G. *Phys. Rev. B* **2007**, *75*, 045121.
(27) Fuggle, J. C.; Hillebrecht, F. U.; Zolnierek, Z.; Lasser, R.; Freiburg, C.; Gunnarsson, O.; Schonhammer, K. *Phys. Rev. B* **1983**, *27*, 7330–7341.
(28) Thompson, A.; Attwood, D.; Gullikson, E.; Howells, M.; Kim, K.; Kirz, J.; Kortright, J.; Lindau, I.; Pianetta, P.; Robinson, A.; Scofield, J.; Underwood, J.; Vaughan, D.; Williams, G.; Winick, H. *X-ray Data Booklet*, 2nd ed.; Lawrence Berkeley National Laboratory: Berkeley, CA, 2001.
(29) Yang, Z. X.; Lu, Z. S.; Luo, G. X. *Phys. Rev. B* **2007**, *76*, 75421.
(30) Alfredsson, M.; Catlow, C. R. A. *Phys. Chem. Chem. Phys.* **2002**, *4*, 6100–6108.
(31) Freund, H. J. *Surf. Sci.* **2007**, *601*, 1438–1442.
(32) Pacchioni, G.; Giordano, L.; Baistrocchi, M. *Phys. Rev. Lett.* **2005**, *94*, 226104.

JP8004103